Sustainable Energy, Grids and Networks 4 (2015) 16–28

Contents lists available at ScienceDirect

Sustainable Energy, Grids and Networks

journal homepage: www.elsevier.com/locate/segan

Using PMU signals from dominant paths in power system wide-area damping control

Yuwa Chompoobutrgool [a,*], Luigi Vanfretti [a,b]

[a] KTH Royal Institute of Technology, Stockholm, Sweden
[b] Statnett SF, Research & Development, Oslo, Norway

ARTICLE INFO

Article history:
Received 9 March 2015
Received in revised form
29 June 2015
Accepted 9 September 2015
Available online 9 October 2015

Keywords:
Wide-area damping control
Time delays
Synchronized phasor measurements
Inter-area oscillations
Dominant inter-area oscillation paths
Delay margin

ABSTRACT

This article presents a comprehensive study of dominant inter-area oscillation path signals and their application for power system wide-area damping control (WADC). The analysis, carried out on both small and large study systems, focuses on the relationships that emerge from physical characteristics of inter-area oscillations, namely the modal observability of signals from dominant paths and their corresponding control loop system properties (i.e. stability and robustness). The aim is to be able to appropriately exploit the dominant path signals for the mitigation of inter-area oscillations. Guidelines and considerations are provided to facilitate the design of WADC using the proposed approach.

© 2015 The Authors. Published by Elsevier Ltd.
This is an open access article under the CC BY-NC-ND license (http://creativecommons.org/licenses/by-nc-nd/4.0/).

1. Introduction

Motivation

In response to a continual increase in electricity demand and the trend for more interconnections [1], power systems are driven closer to their physical operation limits, especially those of transmission capacity. Consequently, one critical issue concerning security and reliability of power system operation is the mitigation of inter-area oscillations. Various approaches for damping control design have been investigated in previous works [2–5]. Among different damping devices, power system stabilizers (PSS) are the most commonly used.

The advent of phasor measurement units (PMU) makes possible the use of remote or *wide-area* signals which enables various applications. Of significance is the wide-area damping control (WADC) application which utilizes remote measurements from PMUs to increase damping of the inter-area oscillations. It has been suggested that wide-area control can be more effective than local control [2,3,5] thanks to their larger observability of the inter-area modes. This makes the exploitation of PMU signals desirable for damping control purposes. One of the major challenges in WADC design is, however, the selection of feedback input signals. Which remote signal would give a satisfactory or the most effective damping performance?

Previous work

Among all available PMU signals,[1] [6] presents a systematic approach using the concept *dominant inter-area oscillation paths* to select feedback input signals having highest open-loop observability. The term *network modeshape*, a variable used to characterize the dominant path, has a commensurate relationship with damping effectiveness, i.e., the larger the network modeshape a signal has, the higher damping ratio the system can achieve. This relationship has been demonstrated in [7], where it has been shown that damping performance of a system corresponds to the network modeshape content of the selected feedback input.

Another challenge with WADC design is latency handling. Recently, many power system studies have considered fixed time delays where Padé approximation is used to represent them [8,9,3] whereas time-varying delays have also been investigated in several works including [10–12]. Regardless of their representation, deterministic or stochastic, time delays have detrimental impacts on system performance and can lead to loss of synchronism or instability [13]. As such, to implement PMU measurements

* Corresponding author.
E-mail address: yuwa@kth.se (Y. Chompoobutrgool).

[1] Voltage and current phasors, i.e., voltage and current magnitude and angles.

http://dx.doi.org/10.1016/j.segan.2015.09.001
2352-4677/© 2015 The Authors. Published by Elsevier Ltd. This is an open access article under the CC BY-NC-ND license (http://creativecommons.org/licenses/by-nc-nd/4.0/).

for WADC, time delays, together with their impacts on control performance and system stability, must be carefully investigated.

The study in [14] presents preliminary studies on different properties of control systems using dominant path signals. The main finding is the trade-off between damping capacity and the maximum allowable delay the system can accommodate, i.e. delay margin. Relationship between delay margin and WADC parameters has been investigated in [12] where a method to compute delay margin is proposed. Since delay margin determines system stability, it can be used as a metric for WADC design.

Objectives

The objective of this article is twofold: (i) to provide a comprehensive analysis of the relationship between the *network modeshape* and different properties of control loop system (particularly, those related to damping performance, stability and robustness) using dominant inter-area oscillation path signals for WADC design, and (ii) to demonstrate and prove such relationships on a larger power network (since the studies [7,14] were carried out on a small-scale two-area system). With these findings, one can properly use signals from the dominant path in the design of controllers to effectively mitigate inter-area oscillations that constrain power transfer capacity and affect system stability.

Contributions

The contributions of this article are summarized as follows:

- Summary of important relationships (those that are related to stability and robustness) of control loops using dominant inter-area oscillation path signals as feedback inputs.
- Realization of the dominant inter-area oscillation path concept on a large power system.
- A metric and guideline for WADC design.

Paper organization

The paper is organized as follows. Section 2 introduces important concepts and summarizes major findings in preceding works by the authors. In Section 3, study system descriptions and case studies are described. Section 4 presents the main findings of this work, i.e., the relationships between control loop properties and network modeshape of the dominant path signals. Section 5 provides the verification of the designed controllers and delay margins through nonlinear time-domain simulations while in Section 6 the properties of a large system are demonstrated. Section 7 discusses some practical considerations and proposes some guidelines for WADC design while in Section 8, comparative analysis on different signal selection approaches are presented. Conclusions are presented in Section 9.

2. Basis of study

This section introduces important concepts used throughout the study and summarizes major findings in preceding works.

2.1. Important concepts

- *Interaction paths* are defined as the group of transmission lines, buses, and controllers which the generators in a system use for exchanging energy during swings [15].
- *Dominant inter-area oscillation paths* are defined as the interaction paths containing the highest content of the inter-area mode. They are pinpointed by network modeshape of signals on the dominant paths. These network modeshapes have certain features which are deterministic [6].
- *Network modeshapes (S)* are the projection of the network sensitivities (C) onto the modeshape (Φ) and are computed from the product of the two terms. They indicate how much of the content of each mode is distributed within the network variables. The network variables of interest are voltage phasors, i.e., voltage magnitude and angles. Thus, their corresponding network modeshapes are represented by S_V and S_θ, respectively. The mathematical expressions of the network modeshapes are provided below.

Suppose the linearized model of an N-machine power system can be given in a state-space form as

$$\Delta\dot{x}_P = A_P\Delta x_P + B_P\Delta u_P \tag{1}$$

$$\Delta y_P = C_P\Delta x_P + D_P\Delta u_P, \tag{2}$$

where A_P is the system matrix, B_P the input matrix, C_P the output matrix, D_P the feedforward matrix, x_P the state vector, u_P the control vector, and y_P the output vector.

Assuming $u_P = 0$, the model is expressed as

$$\underbrace{\begin{bmatrix}\Delta\dot{\delta}\\ \Delta\dot{\omega}\\ \Delta\dot{z}\end{bmatrix}}_{\Delta\dot{x}} = \underbrace{\begin{bmatrix}A_{11} & A_{12} & A_{13}\\ A_{21} & A_{22} & A_{23}\\ A_{31} & A_{32} & A_{33}\end{bmatrix}}_{A}\underbrace{\begin{bmatrix}\Delta\delta\\ \Delta\omega\\ \Delta z\end{bmatrix}}_{\Delta x} \tag{3}$$

where matrix A represents the state matrix corresponding to the state variables $\Delta\delta$, $\Delta\omega$, and Δz. Elements in z refer to other state variables. Then, performing eigenanalysis, the mode shape is derived from

$$A\Phi = \lambda\Phi \tag{4}$$

where λ are eigenvalues of the system and $\Phi = [\Phi_1\Phi_2\cdots\Phi_n]$ are the corresponding right eigenvectors (or mode shapes) and n is the number of state variables. Inter-area oscillations, as well as other modes, are determined from the eigenvalues.

The sensitivities of interest are the bus voltage phasors with respect to change in the state variables, e.g. machine's rotor angle (δ) or speed (ω). That is, the network sensitivities are the C_P matrix from Eq. (2) with voltage magnitude (V) and angle (θ) as the outputs, Δy.

Sensitivities of the voltage magnitude (C_V) and angle (C_θ) are expressed as

$$I\underbrace{\begin{bmatrix}\Delta V\\ \Delta\theta\end{bmatrix}}_{\Delta y} = \underbrace{\begin{bmatrix}\frac{\partial V}{\partial\delta} & \frac{\partial V}{\partial\omega} & \frac{\partial V}{\partial z}\\ \frac{\partial\theta}{\partial\delta} & \frac{\partial\theta}{\partial\omega} & \frac{\partial\theta}{\partial z}\end{bmatrix}}_{C}\underbrace{\begin{bmatrix}\Delta\delta\\ \Delta\omega\\ \Delta z\end{bmatrix}}_{\Delta x} = \begin{bmatrix}C_V\\ C_\theta\end{bmatrix}\begin{bmatrix}\Delta\delta\\ \Delta\omega\\ \Delta z\end{bmatrix} \tag{5}$$

$$C_V = \begin{bmatrix}C_{V\delta} & C_{V\omega} & C_{Vz}\end{bmatrix},$$

$$C_\theta = \begin{bmatrix}C_{\theta\delta} & C_{\theta\omega} & C_{\theta z}\end{bmatrix}.$$

Then, the expressions for voltage magnitude and angle modeshapes, S_V and S_θ, are

$$S_V = C_V\Phi, \qquad S_\theta = C_\theta\Phi. \tag{6}$$

- *Delay margin (DM)* is defined as the smallest time required to destabilize the closed-loop system [16]. It can be computed from the following. Fig. 1 shows a feedback connection of three systems: a plant $G(s)$, a controller $H(s)$, and a time delay $TD(s)$. The time delay is represented by a 2nd-order Padé approximation:

$$TD(s) \approx \frac{12 - 6sT_d + T_d^2s^2}{12 + 6sT_d + T_d^2s^2}, \tag{7}$$

where T_d represents time delay in second.

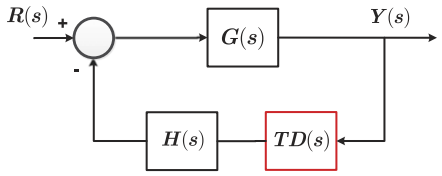

Fig. 1. Block diagram of a feedback connection.

Let $L(s)$ be the series product of $G(s)$ and $H(s)$, i.e. $L(s) = G(s)H(s)$. Assume that for $TD(s) = 1$ (no delay), the closed-loop system is stable. Then, when a delay is added to the loop, the open-loop transfer function including time delay has the form $L(s)TD(s)$. Let ω_c be the gain crossover frequencies, the frequencies at which the magnitude of the transfer function $|L(j\omega_c)TD(j\omega_c)| = 1$, i.e., crosses 0 dB. Then, the T_d that obtains from $\angle L(j\omega_c)TD(j\omega_c) = -180^\circ$ is defined as delay margin, the time delay that makes the closed-loop system become unstable.

- *Sensitivity function (Sn(s))*
  Assume $TD(s) = 1$ (no delay). The closed-loop transfer function from $R(s)$ to $Y(s)$ of the feedback connection in Fig. 1 can be expressed as

$$T(s) = \frac{Y(s)}{R(s)} = \frac{G(s)}{1 + G(s)H(s)}. \tag{8}$$

By separating a gain K from the controller transfer function, the controller can be expressed as $H(s) = KF(s)$. Then, the change of $T(s)$ with respect to a change of K is defined as the sensitivity function [17]

$$Sn(s) = \frac{\partial T(s)/T(s)}{\partial K/K} = \frac{1}{1 + G(s)KF(s)} = \frac{1}{1 + G(s)H(s)}. \tag{9}$$

The magnitude of sensitivity function evaluated at frequency ω_n, $|Sn(j\omega_n)|$, indicates the robustness of the feedback system with respect to the variations of K at that frequency.

2.2. Summary of previous findings

- The dominant inter-area oscillation path concept pinpoints the signals having the largest modal observability of the inter-area mode of interest within the network [6].
- There is a degree of persistence to the existence of the dominant path; i.e., it will be consistent under various operating conditions (provided that the changes are small) [18].
- Damping performance of a system corresponds to the network modeshape of the feedback input. In other words, signals having high network modeshape achieve higher damping ratios than those with lower network modeshapes [7]. The study in [7] was carried out on a two-area single radial system having 5 buses. According to the study, voltage angle difference is the most effective damping signal comparing to voltage magnitude and generator rotor's speed.
- There is a trade-off between damping performance and delay margin [14].

3. Study system

3.1. System description

The system of study is illustrated in Fig. 2 where G_1, G_2, and G_3 represent the main clusters of machines involved in the inter-area oscillations between Areas C, B, and A, respectively. G_1 is connected to Slack bus (Bus 1) and its dynamic is described by using a classical model while those of G_2 and G_3 are 3rd-order model. Exciters represented by 3 states are connected at G_2 and G_3. Note that the system data is modified from [19].

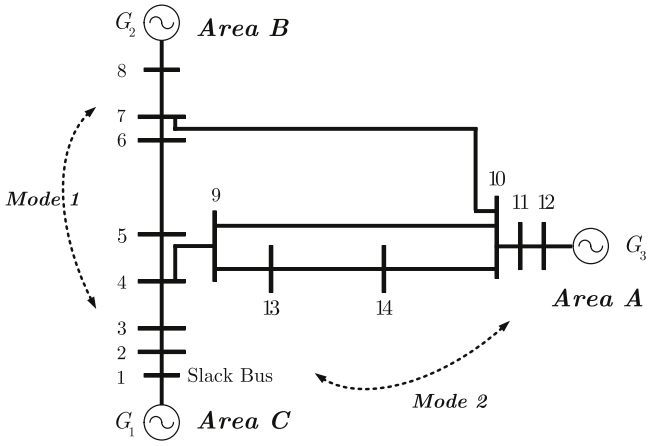

Fig. 2. The three-area study system.

Table 1
Eigenanalysis of the three-area system.

System ($P_{8,1}$)	Mode	Area	λ_i	Freq. (Hz)	ζ_i (%)
Low (0.2)	1	B↔C	$-0.06 \pm j1.76$	0.28	3.60
	2	A↔C	$-0.13 \pm j2.57$	0.41	5.07
Medium (0.5)	1	B↔C	$-0.07 \pm j1.65$	0.26	4.03
	2	A↔C	$-0.13 \pm j2.48$	0.39	5.31
High (0.8)	1	B↔C	$-0.07 \pm j1.14$	0.18	6.36
	2	A↔C	$-0.13 \pm j2.29$	0.36	5.75

3.2. Case studies and small-signal stability analysis

Three different operating conditions have been constructed, namely, *Low*, *Medium*, and *High* by varying the active power flow from Bus 8 to Bus 1. The *Medium* system having active power flow $P_{8,1} = 0.5$ pu is defined as the *nominal* operating condition case from here on. For each operating condition, small signal stability analysis has been carried out by performing eigenvalue analysis. Two poorest damping modes for each case are summarized in Table 1.[2]

In all cases, there are two dominant inter-area modes of oscillations, namely Mode 1 and Mode 2. Although for the ease of demonstration we consider only the damping performance of Mode 1, the methods and analysis are generic and applicable to any other inter-area mode damping studies.

3.3. Dominant inter-area oscillation paths

By implementing the model-based algorithm in [6], the origin of Mode 1 is found to be starting from G_2 (which is connected to Bus 8) in Area B and continuing down towards area C through Buses 7, 6, 5, 4, 3, 2 and ends at Bus 1. These buses constitute the dominant inter-area oscillation path of Mode 1.

Voltage magnitude and voltage angle modeshapes (S_V and S_θ) for the three case studies are illustrated in Fig. 3. The x-axis represents the bus number in the dominant path; the distance between buses are proportional to the line impedance magnitude. The results comply with [6] that the largest S_θ can be obtained from

[2] An explanation of the relationship between damping performance and loading levels is given in the Appendix.

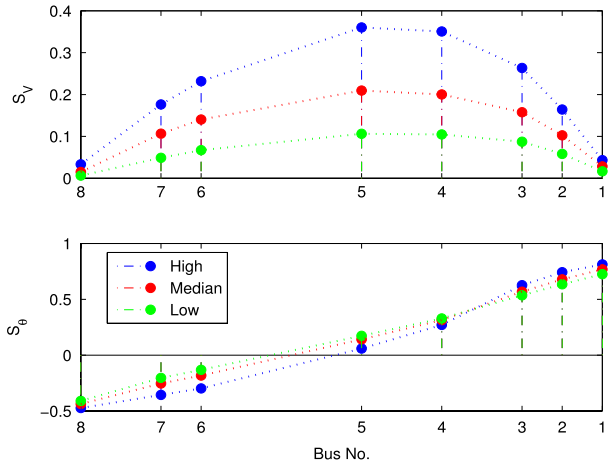

Fig. 3. Mode 1's network modeshapes: comparison among 3 operating conditions.

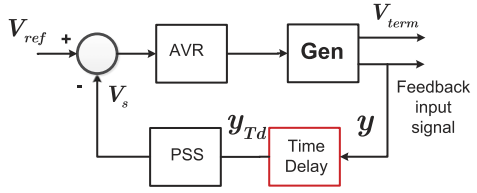

Fig. 4. Block diagram of the study system.

taking the differences between the two edges of the path and inter-area contents of the network modeshapes are more observable in a more stressed system.

Thus, it is expected that using a signal having the largest network modeshape within a dominant path e.g. $\Delta\theta_{1,8}$ should yield the best damping performance than using any other signals within the system.

4. Properties of dominant path signals

From here onwards, we only consider voltage angle differences, $\Delta\theta_{ij}$, as feedback input signals due to its superior effectiveness over voltage magnitude and speed signals.[3] The simulation studies are carried out by using MATLAB/SIMULINK and PSAT.

The block diagram of the study system is illustrated in Fig. 4. Note that the power system stabilizer (PSS) block also includes washout and torsional filters.

4.1. Open-loop properties: no PSS

Properties of the open-loop systems measured at y (see Fig. 4) in frequency domain having dominant path signals as feedback inputs are summarized in Table 2. Abbreviations *GIF* and *PIF* refer to gain and phase measured at the inter-area frequency, respectively. Zero locations refer to the zeros that are closest to the inter-area mode. It is desirable for the zeros to be far from the inter-area mode [20]. Signal $\Delta\theta_{10,8}$ is used to represent a signal from a non-dominant path. Note that in the first column, all voltage angle signals are the differences between the denoted signal and the reference signal (θ_8). In addition, they are presented in ascending order of their distances to the PSS site (Bus 8), from Bus 7 to Bus 1 (except for $\Delta\theta_{10,8}$). These results aid to demonstrate the properties of the modal observability of the network variables (the voltage angle differences), therefore, the PSS is not yet included in the transfer function.

Table 2
Open-loop system properties: No PSS.

Signals	$S_{\Delta\theta}$	*GIF*	*PIF* (deg)	Zero locations
$\Delta\theta_{7,8}$	0.18	0.16	−188.53	$-0.09 \pm j2.97$
$\Delta\theta_{6,8}$	0.25	0.22	−188.63	$-0.08 \pm j2.98$
$\Delta\theta_{5,8}$	0.58	0.49	−189.72	$-0.07 \pm j3.80$
$\Delta\theta_{4,8}$	0.75	0.64	−190.34	$-0.08 \pm j5.67$
$\Delta\theta_{3,8}$	1.01	0.86	−190.75	$-0.12 \pm j15.71$
$\Delta\theta_{2,8}$	1.12	0.95	−190.98	None
$\Delta\theta_{1,8}$	1.21	1.03	−191.22	None
$\Delta\theta_{10,8}$	0.57	0.49	−191.05	None

According to Table 2, the network modeshapes of the dominant path signals, $S_{\Delta\theta}$, are directly proportional to *GIF* [14], which also determines the damping capacity. *PIF*, together with the zero locations, is proportional to the electrical distance from the controller and determines how much phase compensation a controller requires while the distance to the zero can be used as preference of the signal.

In the following, properties of the dominant path signals are illustrated through a design of wide-area damping controller, i.e., a PSS that utilizes PMU signals as input. The objective is to improve damping of the inter-area Mode 1 of the study system using wide-area signals from the dominant path. Two studies are performed: (i) fixed PSS and (ii) retuned PSS, and are demonstrated only with the nominal (*Medium*) operating condition.

The PSS is connected at G_2 (where the origin of Mode 1 is). Voltage angle difference signals ($\Delta\theta_{i,ref}$) along the dominant path of Mode 1 will be fed back in the control loop where θ_8 is the reference. The design procedure for the PSS follows [7].

4.2. Fixed PSS

In practice, PSS structures are generally fixed and so is the feedback signal. By fixing the structure of the PSS and applying signals on the dominant path as feedback inputs y (see Fig. 4), properties of dominant path signals in frequency – as well as time – domains can be investigated. This study mimics the situation when the primary feedback signal (the one originally used for the controller's design) is not available, and another PMU signal is used as backup.

The fixed PSS parameters used are the one that are designed when signal $\Delta\theta_{1,8}$ is the feedback input. The controller gain is selected such that the damping ratio of Mode 1 is equal to 15% for this signal.

4.2.1. Frequency-domain performance

Bode and root locus plots of the open-loop system including the PSS output at V_s (in Fig. 4) using dominant path signals are illustrated in Fig. 5(a)–(b), respectively. Time delay is not yet included. In Fig. 5(a), the dashed arrow pinpoints the magnitude at Mode 1's frequency which are proportional to their respective network modeshapes. The dashed arrow in Fig. 5(b) is in the direction of increasing network modeshape of the feedback signals (and also increasing the distances between the controller and the input signal locations). 'x' mark denotes the point where the gain was selected for each closed-loop system. It is, thus, clear that the larger the network modeshape a signal has, the higher the damping ratio that can be achieved (for the same value of gain) [7].

Properties of the closed-loop systems with dominant path signals in frequency and time domains are summarized in Table 3. They are gain margin (GM) in dB, phase margin (PM) in degree, delay margin (DM), magnitude of the sensitivity function $|Sn(j\omega_n)|$

[3] See [7] for comparison between voltage magnitude, voltage angle difference, and speed as input signals.

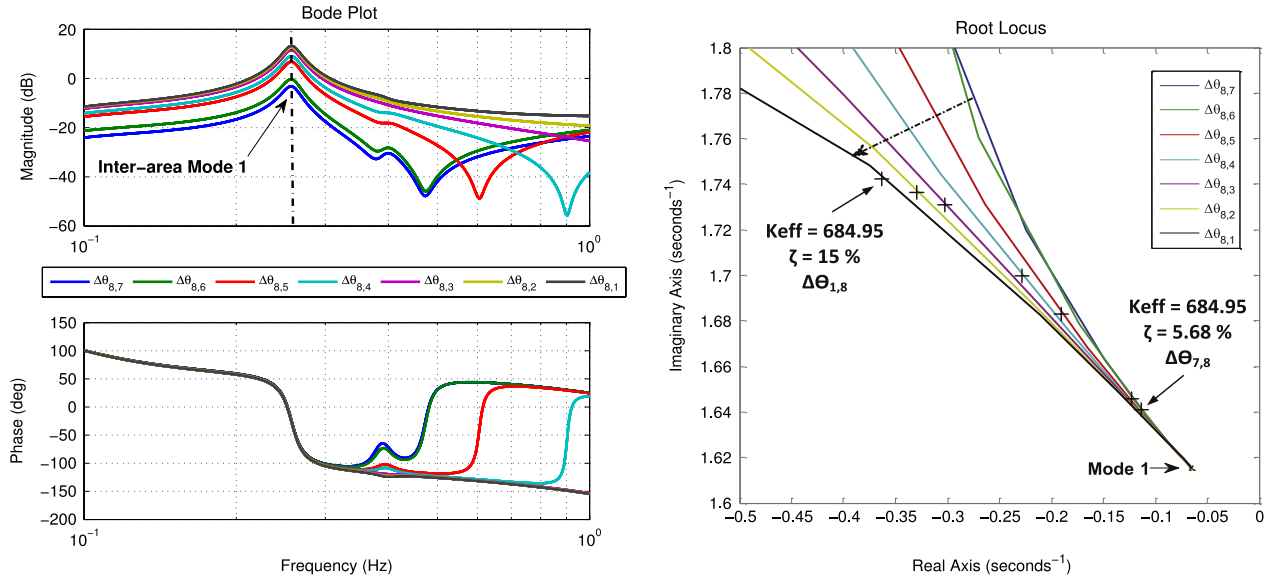

(a) Bode plots.

(b) Root locus plots.

Fig. 5. Bode and root locus plots of dominant path signals: fixed PSS.

Table 3
Control loop metrics: Fixed PSS.

Signals	GM	PM	DM (ms)	$\lvert Sn(j\omega_n)\rvert$	ζ_{m1} (%)	M_p (%)	t_r (s)
$\Delta\theta_{7,8}$	32.53	N/A	N/A	0.69	5.68	17.45	2.47
$\Delta\theta_{6,8}$	29.98	N/A	N/A	0.62	6.30	17.87	2.49
$\Delta\theta_{5,8}$	29.06	107.87	1117.3	0.41	9.12	19.21	2.55
$\Delta\theta_{4,8}$	34.97	95.23	965.3	0.35	10.68	19.59	2.57
$\Delta\theta_{3,8}$	35.41	85.39	840.8	0.28	13.00	20.12	2.61
$\Delta\theta_{2,8}$	23.94	82.29	800.0	0.26	14.06	20.24	2.62
$\Delta\theta_{1,8}$	18.60	80.01	769.2	0.25	15.00	20.27	2.63
$\Delta\theta_{10,8}$	23.26	105.88	1095.7	0.42	9.22	18.67	2.54

N/A: Since the magnitude responses do not cross 0 dB, there is no gain crossover frequency, thus no PM nor DM.

evaluated at ω_n (the inter-area frequency),[4] damping ratio (ζ_{m1}), overshoot (M_p), and rise time (t_r). The former three margins indicate the relative stability of a feedback system while $|Sn(j\omega_n)|$ indicates the robustness of the system with respect to a variation in the controller gain [17] at the inter-area frequency.

From the results in the table, it can be summarized that (i) PM, DM, and $|Sn(j\omega_n)|$ are inversely proportional to $S_{\Delta\theta}$ (see Table 2), (ii) ζ_{m1}, M_p, and t_r are proportional to $S_{\Delta\theta}$, and (iii) there is no explicit relationship between GM and $S_{\Delta\theta}$ but they have, to some extent, an inverse relationship. Then, when the PSS parameters are fixed, the following relationships between certain properties and the dominant path signals can be deduced:

- The larger $S_{\Delta\theta}$ a signal has, the higher the damping capacity the system can achieve and the higher the robustness to the controller's gain variation.
- Yet, the larger $S_{\Delta\theta}$ a signal has, the larger the overshoot and the rise time are and the smaller the stability margins (phase and delay margins) become.

These results corroborate the findings in [7] that the damping performance is proportional to the input signal's modal observability and the findings in [14] that there is a trade-off between damping performance and delay margin.

[4] From here onwards, when referring by sensitivity, it is the sensitivity function evaluated at the frequency of Mode 1.

Table 4
Loading effects: Comparison among three operating conditions, fixed PSS.

Signals	ζ_{m1} (%)			DM (ms)			$\lvert Sn(j\omega_n)\rvert$		
	L	*M*	*H*	*L*	*M*	*H*	*L*	*M*	*H*
$\Delta\theta_{7,8}$	4.40	5.68	8.87	N/A	N/A	N/A	0.81	0.69	0.70
$\Delta\theta_{6,8}$	4.69	6.30	10.05	N/A	N/A	N/A	0.76	0.62	0.60
$\Delta\theta_{5,8}$	5.86	9.12	16.62	N/A	1117.3	1437.7	0.60	0.41	0.33
$\Delta\theta_{4,8}$	6.47	10.68	20.39	N/A	965.3	1213.4	0.54	0.35	0.26
$\Delta\theta_{3,8}$	7.25	13.00	26.61	1195.2	840.8	991.6	0.47	0.28	0.20
$\Delta\theta_{2,8}$	7.63	14.06	28.84	1104.9	800.0	932.0	0.45	0.26	0.18
$\Delta\theta_{1,8}$	7.99	15.00	30.35	1042.7	769.2	894.6	0.43	0.25	0.17

Comparing between signals $\Delta\theta_{5,8}$ and $\Delta\theta_{10,8}$ which have about the same network modeshapes, they both yield similar performance in damping but the dominant signal can accommodate larger delay than the non-dominant signal. Depending on system's requirements or signal availability, one may choose one signal over the other.

4.2.2. Time responses of the dynamic system and its performance

A 1% step change is applied at the voltage reference, V_{ref}, of the exciter at G_2. The time responses of the closed-loop systems are illustrated in Fig. 6(a)–(b) for terminal voltage variation at Bus 8, ΔV_8, and active power variation at Bus 8, ΔP_8, respectively. As expected, Mode 1 is the least damped with the signal $\Delta\theta_{7,8}$ while is the most damped with the signal $\Delta\theta_{1,8}$ as feedback inputs.

4.2.3. Loading effects

To investigate the impact of changes in power flow in the dominant path on the signal properties and to corroborate the relationship found in previous sections, the same studies are implemented with two other operating conditions. For all cases, the same PSS structures (the one designed for the nominal operating condition) are used. The damping performance, delay margins, and sensitivity are summarized in Table 4. Abbreviations *L*, *M*, and *H* stand for the three operating conditions: *Low*, *Medium*, and *High*, respectively.

Regardless of the operating condition, the behaviors of ζ_{m1}, DM, and $|Sn(j\omega_n)|$ comply with the dominant inter-area oscillation path concept. That is, ζ_{m1} is proportional to $S_{\Delta\theta}$ while DM and $|Sn(j\omega_n)|$ are inversely proportional to it.

Comparing among the three scenarios, it can be seen that the *High* case achieves the highest damping ratios followed by the

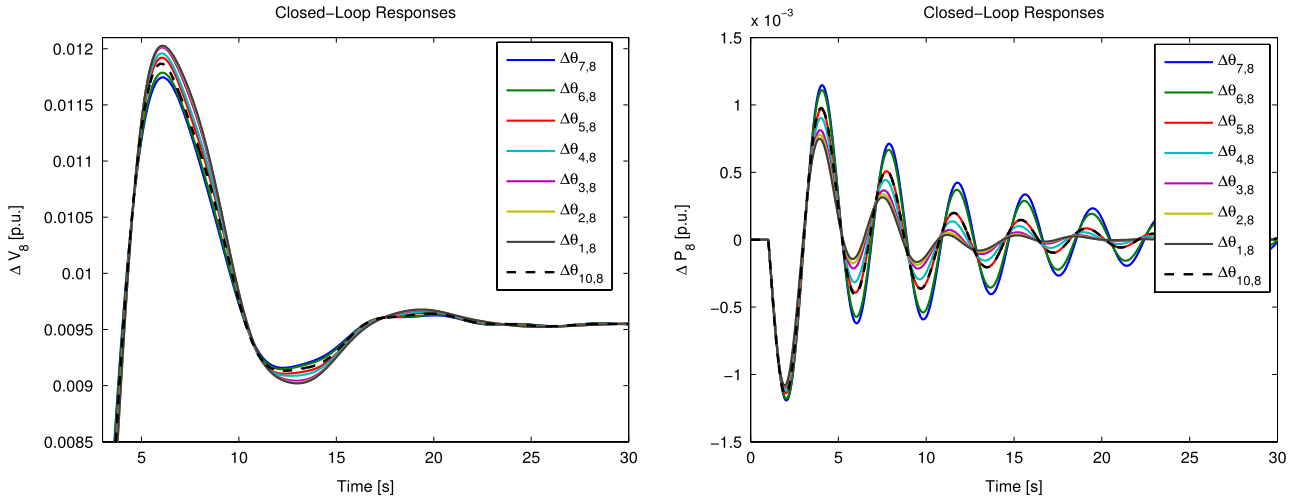

(a) Terminal voltage variation at Bus 8.

(b) Active power variation at Bus 8.

Fig. 6. Time responses of the closed loop system, fixed PSS.

Medium and the *Low* cases, respectively. This could be due to the inverse relationship between synchronizing coefficient (K_S) and damping ratios.[5] By computing from the A matrix of each case, the norm of synchronizing coefficient $|K_S|$ of all three cases has the relationship $|K_{S,High}| < |K_{S,Medium}| < |K_{S,Low}|$. Thus, their corresponding damping ratios follow in a reverse order. See Appendix for the derivation of the relationship. Note that this relationship is valid here because the generators are modeled with low orders. For more complex models, this relationship may not hold.

As for the delay margin, no definite conclusion can be drawn for the relationship between the property and the system's loadings since delay margin is generally dependent on the system's gain-crossover frequency rather than the system's condition.

As for the sensitivity function, the system is more sensitive (less robust) to the changes in controller gain as the stress in the system is reduced.

4.3. Retuned PSS

Generally, a PSS is designed to meet certain specifications and, therefore, each feedback signal requires different PSS parameters. In this section, the purpose of the design is to achieve a specific damping performance. As such, for each input signal, PSS parameters and gain will be tuned such that the damping ratio of Mode 1 $\zeta_{m1} = 15\%$. This method could facilitate the future online implementation of WADC when feedback input can be selective and controller parameters can be adjustable. Relationships between signals' network modeshapes and signal properties are drawn.

4.3.1. Frequency-domain performance

Bode and root locus plots of the open-loop system at V_s (see Fig. 4) using dominant path signals are illustrated in Fig. 7(a)–(b), respectively.

The magnitude and phase at the inter-area frequency of the Bode plot in Fig. 7(a) are nearly the same for all signals. The dashed line in Fig. 7(b) indicates damping value of 15%. It can be seen that to achieve the same damping performance, a signal with larger network modeshape requires smaller values of gain. This emphasizes the benefit of using a signal with large network modeshape.

From the results of properties of the closed-loop system in Table 5, it can be summarized that (i) PM, DM, K_{eff} (the effective gain), M_p, and t_r are inversely proportional to $S_{\Delta\theta}$, (ii) $|Sn(j\omega_n)|$ is proportional to $S_{\Delta\theta}$, and (iii) GM are larger when signals from the center of the dominant path are used than signals from the edges. Then, for the same damping performance, the following relationships between certain properties and the dominant path signals can be deduced:

- The larger $S_{\Delta\theta}$ a signal has, the smaller the gain required to achieve the same damping performance and the smaller overshoot and rise time become.
- Yet, the larger $S_{\Delta\theta}$ a signal has, the lower the robustness to controller's gain variation and the smaller the stability margins (phase and delay margins) become.

These results corroborate the findings in [7] that using a signal having higher modal contents requires smaller gain, thus less susceptible to noise, but at the same time, results in having smaller delay margin [14], and more sensitive to variation in the controller gain.

Table 5
Control loop metrics: Retuned PSS.

Signals	GM	PM	DM (ms)	$\|Sn(j\omega_n)\|$	K_{eff}	M_p (%)	t_r (s)
$\Delta\theta_{7,8}$	14.05	82.25	785.9	0.20	5598	23.71	2.70
$\Delta\theta_{6,8}$	14.48	82.19	785.8	0.21	3975	23.52	2.70
$\Delta\theta_{5,8}$	21.73	81.42	782.1	0.23	1566	21.98	2.66
$\Delta\theta_{4,8}$	30.34	80.87	777.8	0.24	1153	21.26	2.65
$\Delta\theta_{3,8}$	33.54	80.46	774.0	0.24	841	20.77	2.64
$\Delta\theta_{2,8}$	23.14	80.26	771.9	0.25	749	20.51	2.63
$\Delta\theta_{1,8}$	18.60	80.01	769.2	0.25	685	20.27	2.63
$\Delta\theta_{10,8}$	16.62	80.33	772.5	0.24	1440	20.57	2.64

4.3.2. Loading effects

Similar to the fixed PSS study, comparisons among the three operating conditions are made. The PSS structures are adjusted to each individual system (feedback input signal and operating condition) to meet the desired damping ratio of 15%. The effective gain, delay margin, and sensitivity function comparisons are summarized in Table 6.

For every operating condition, the behaviors of K_{eff}, DM, and $|Sn(j\omega_n)|$ comply with the results in Table 5. With the exception of the *Low* scenario where the DM is proportional to $S_{\Delta\theta}$.

Comparing among the three operating conditions, it can be seen that the higher the power flow, the lesser the K_{eff} that it is required. This relates to their corresponding $S_{\Delta\theta}$ (see the bottom figure of Fig. 3). From Table 2, there is a linear relationship between $S_{\Delta\theta}$ and

[5] This relationship is valid for a second-order system.

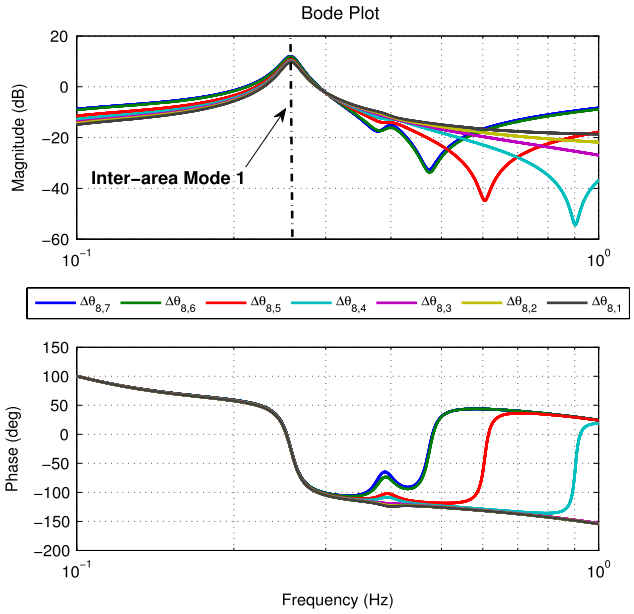

(a) Bode plots.

(b) Root locus plots.

Fig. 7. Bode and root locus plots of dominant path signals: retuned PSS.

Table 6
Loading effects: Comparison among three operating conditions, retuned PSS.

Signals	K_{eff}			DM (ms)			$\lvert Sn(j\omega_n)\rvert$		
	L	*M*	*H*	*L*	*M*	*H*	*L*	*M*	*H*
$\Delta\theta_{7,8}$	11 800	5598	2367	659.0	785.9	1729.5	0.21	0.20	0.37
$\Delta\theta_{6,8}$	9057	3975	1512	665.8	785.8	1725.2	0.20	0.21	0.37
$\Delta\theta_{5,8}$	4231	1566	457	670.3	782.1	1712.4	0.21	0.23	0.40
$\Delta\theta_{4,8}$	3210	1153	321	667.9	777.8	1705.6	0.21	0.24	0.41
$\Delta\theta_{3,8}$	2602	841	211	681.9	774.0	1693.6	0.21	0.24	0.41
$\Delta\theta_{2,8}$	2355	749	190	684.8	771.9	1691.2	0.21	0.25	0.41
$\Delta\theta_{1,8}$	2146	685	179	686.1	769.8	1688.2	0.21	0.25	0.42

GIF from the magnitude of Bode plot. For the same feedback signal, *GIF* is largest in the *High* case and smallest in the *Low* case. This implies that, to achieve the same damping performance, the gain is least required in the *High* case and vice versa.

As for the delay margin, the results in the table imply that DM corresponds to the stress of the system: the higher the stress of a system, the larger delay it can accommodate. However, as stated previously, DM is more dependent on the gain-crossover frequency than the modal observability of the input signals. Thus, this relationship may not hold in some other cases.

Additionally, regardless of the case, the variations in DM among the dominant path signals are much smaller for the retuned PSS than the fixed PSS.

As for the sensitivity, the results are opposite to the fixed PSS study. Here, $|Sn(j\omega_n)|$ increases as $S_{\Delta\theta}$ increases which is a trade-off for requiring low gain.

5. Verification of the results through nonlinear time-domain simulation

Here the results obtained from linear analysis in the previous section are validated using the nonlinear time-domain simulation routine in PSAT.

5.1. Controller damping performance

To validate the performance of the designed controller, small and large disturbances are applied to the study system. The PSS is the one used in Section 4.2 where $\Delta\theta_{1,8}$ is the input signal. The small disturbance is a 1% step change at V_{ref} of the exciter at G_2 (which is the same as in the linear analysis study, see Section 4.2) while the large disturbance is a fault applied at Bus 7 for 125 ms. The time-domain responses are illustrated in Fig. 8(a)–(b), respectively. The blue line represents the system with no control while the green, red, and turquoise lines represent the systems with PSS using signals $\Delta\theta_{1,8}$, $\Delta\theta_{4,8}$, and $\Delta\theta_{7,8}$ (in descending order of $S_{\Delta\theta}$ magnitude) as feedback inputs, respectively. In both studies, the responses are in accordance with the linear analysis results, i.e., using the signal having the largest network modeshape ($\Delta\theta_{1,8}$) yield the best damping performance comparing to using other signals and also without the PSS control.

5.2. Delay margin verification and comparison among dominant path signals

The time delay is modeled using a 2nd-order Padé approximation which represents an end-to-end delay comprising of communication network delays and signal processing delays in Wide-Area Control System (WACS) [21]. For time-delay implementation in PSAT, see [14].

To verify if the delay margin computed from the linearized model will exhibit the same behavior during nonlinear time-domain simulations, the same delay margin together with the same perturbation are implemented in the simulation. The input signal used is the voltage angle differences $\Delta\theta_{1,8}$ which has a delay margin of 769.2 ms. The perturbation used is a 1% step change at V_{ref} of the exciter at G_2. Responses of the active power at Bus 8, P_8, are illustrated in Fig. 9(a). It can be seen that both responses are, despite some small deviations, very close to each other and that the delay margin results in the system being marginally stable. This verifies that the delay margin obtained from the linearized model is valid in the nonlinear domain.

Fig. 9(b) illustrates a property of the dominant path signals when subject to the same disturbance (1% change in V_{ref} of the exciter at G_2) and the same amount of latency (300 ms). The same controller applies to all systems. The damping performance for each signal as feedback inputs corresponds to their respective network modeshape as described in Table 2. The responses

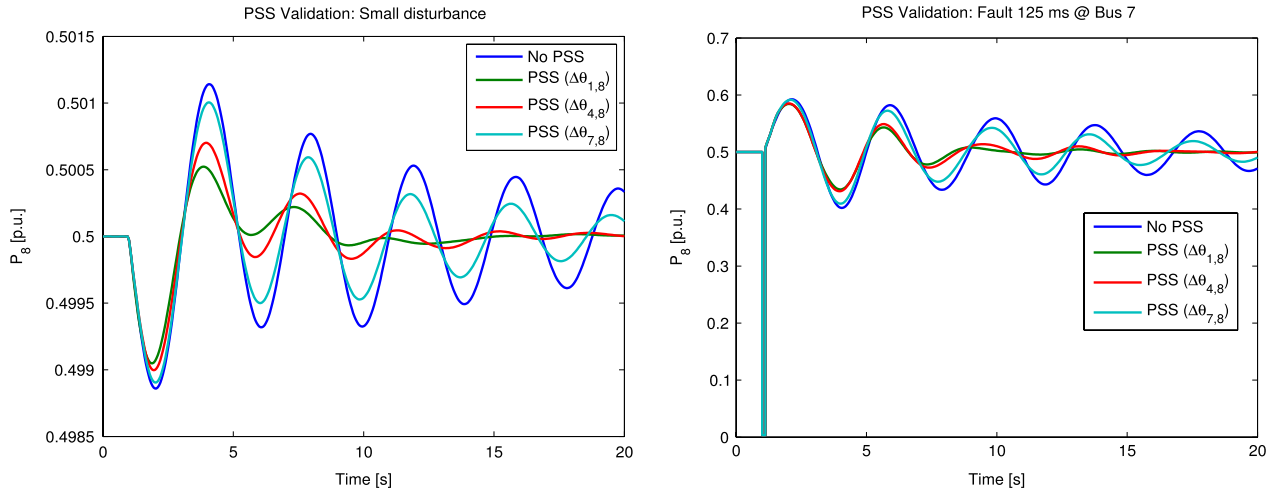

(a) Small disturbance. (b) Large disturbance.

Fig. 8. Validation of PSS performance through disturbances. (For interpretation of the references to color in this figure legend, the reader is referred to the web version of this article.)

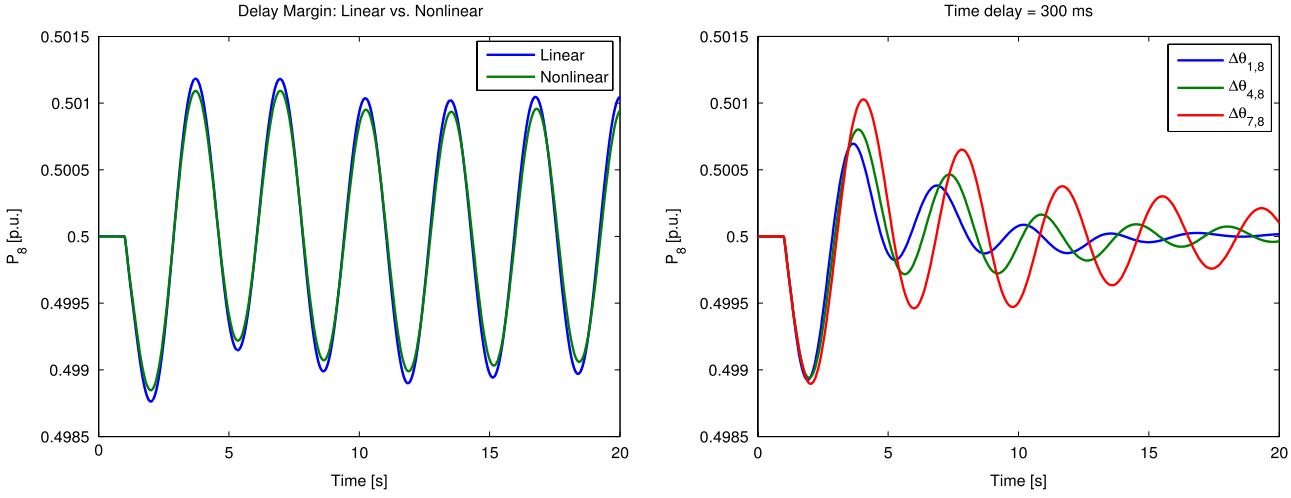

(a) DM verification: linear vs. nonlinear. (b) Dominant path signal comparison.

Fig. 9. DM verification and comparison among dominant path signals.

demonstrate that for the same amount of latency, the signal with larger $S_{\Delta\theta}$ can damp the system better than signal having lower $S_{\Delta\theta}$.

5.3. Time delay compensation

To compensate for the delay, a single-stage phase lead block is added after the PSS [14]. Responses of the system when subject to the same perturbation as in the previous section with and without delay compensation are illustrated in Fig. 10. (Both systems have time delays equal to the delay margin.) From the figure, it can be inferred that if the time delay is known, using a single-stage phase lead block can compensate the phase lag by the delay and, thus, hinder the system from losing its stability.

6. Concept demonstration on a large system

6.1. System description and open-loop properties

To investigate if the relationships found in the 3-area system are applicable to a large interconnected system, the same analysis is carried out on the KTH-NORDIC32 system as illustrated in Fig. 11.

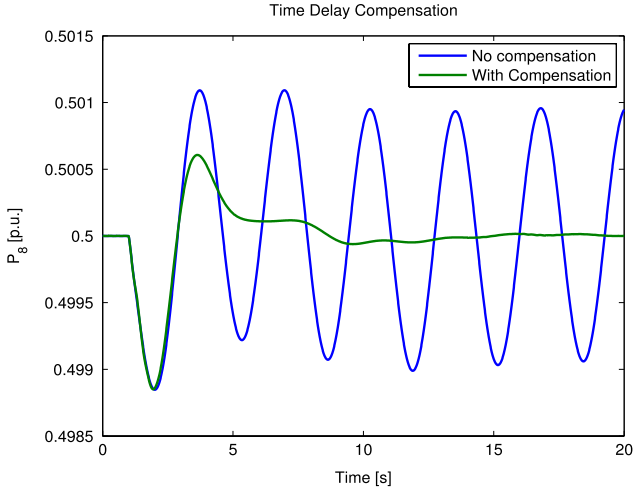

Fig. 10. Time delay compensation.

The system has two lightly damped inter-area modes, 0.49 and 0.72 Hz, whose dominant inter-area oscillation paths are marked

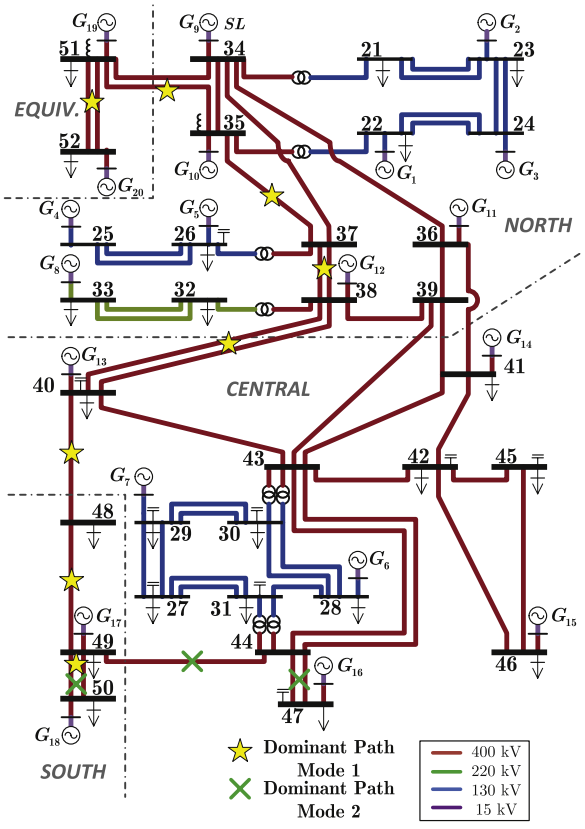

Fig. 11. KTH-NORDIC32 system. (For interpretation of the references to color in this figure legend, the reader is referred to the web version of this article.)

Table 7
Open-loop properties: KTH-NORDIC32.

Signals	$S_{\Delta\theta}$	GIF	PIF
$\Delta\theta_{49,50}$	0.03	2.15	175.75
$\Delta\theta_{48,50}$	0.06	4.42	175.22
$\Delta\theta_{40,50}$	0.14	9.78	174.99
$\Delta\theta_{38,50}$	0.18	13.01	174.86
$\Delta\theta_{37,50}$	0.22	16.17	174.26
$\Delta\theta_{35,50}$	0.24	17.54	173.64
$\Delta\theta_{51,50}$	0.25	17.76	172.23
$\Delta\theta_{52,50}$	0.25	17.93	171.41

by yellow star and green cross, respectively.[6] The generators are represented by 5th- and 6th-orders and include excitation control systems. To constrain the effects of other controls, turbine governors are disconnected from all generators. Similar to previous analysis, only damping of Mode 1 will be demonstrated here.

The dominant inter-area oscillation path of Mode 1 starts from Bus 50 in the South area, continues upward via Buses 49, 48, 40, 38, 37, 35, 51, and ends at Bus 52 in the Equivalent area. Properties of the open-loop systems measured at y (see Fig. 4) having dominant path signals as feedback inputs are summarized in Table 7.

The results in Table 7 are similar to those in Table 2 of the 3-area system. That is, $S_{\Delta\theta}$ of the dominant path signals are proportional to *GIF* while *PIF* is proportional to the distance from the controller. The zero locations are not provided here because for all signals, there are no zeros in close proximity to the inter-area mode.

A PSS is designed to be installed at G_{18} which is connected to Bus 50 and where the origin of Mode 1 is. Voltage angle difference signals ($\Delta\theta_{i,ref}$) along the dominant path will be used as feedback

[6] See [22] for system details and [6] for dominant path identifications.

Table 8
Closed-loop metrics: Fixed PSS, KTH-NORDIC32.

Signals	GM	PM	DM (ms)	$\lvert Sn(j\omega_n)\rvert$	ζ_{m1} (%)	M_p (%)	t_r (s)
$\Delta\theta_{49,50}$	17.07	111.34	627.3	0.3750	2.20	7.74	0.89
$\Delta\theta_{48,50}$	14.51	90.52	501.5	0.2223	3.74	8.83	0.92
$\Delta\theta_{40,50}$	10.77	78.60	419.1	0.1127	7.74	11.06	1.00
$\Delta\theta_{38,50}$	9.93	74.53	387.4	0.0877	10.49	12.65	1.03
$\Delta\theta_{37,50}$	9.72	70.63	357.5	0.0722	13.39	14.36	1.07
$\Delta\theta_{35,50}$	9.80	68.93	345.5	0.0669	14.69	14.95	1.08
$\Delta\theta_{51,50}$	9.68	67.66	339.8	0.0658	14.89	14.82	1.08
$\Delta\theta_{52,50}$	9.61	66.86	336.0	0.0654	15.00	14.77	1.08

Table 9
Closed-Loop metrics: Retuned PSS, KTH-NORDIC32.

Signals	GM	PM	DM (ms)	$\lvert Sn(j\omega_n)\rvert$	K_{eff}	M_p (%)	t_r (s)
$\Delta\theta_{49,50}$	−1.07	−11.20	N/A	0.0646	14 602	N/A	N/A
$\Delta\theta_{48,50}$	2.70	77.31	390.6	0.0594	6 252	15.49	0.99
$\Delta\theta_{40,50}$	5.72	75.68	380.5	0.0620	2 703	13.64	1.04
$\Delta\theta_{38,50}$	7.26	74.18	370.8	0.0636	2 009	14.05	1.06
$\Delta\theta_{37,50}$	8.88	72.22	360.2	0.0661	1 317	14.81	1.07
$\Delta\theta_{35,50}$	9.67	71.04	355.1	0.0725	983	14.97	1.07
$\Delta\theta_{51,50}$	9.66	68.47	343.7	0.0663	646	14.83	1.07
$\Delta\theta_{52,50}$	9.61	66.86	336.0	0.0654	526	14.77	1.07

inputs where θ_{50} is the reference. The structure of the PSS is the same as in Section 4.

6.2. Fixed PSS: frequency-domain properties

The fixed PSS parameters used is the one that is designed when signal $\Delta\theta_{52,50}$ is the feedback signal. The gain is selected such that $\zeta_{m1} = 15\%$ for this signal.

The relationship between system properties and network modeshape are summarized in Table 8. Similar to the 3-area system's results, a signal's network modeshape is proportional to its damping efficacy but inversely proportional to stability margins and robustness to gain variation at the inter-area frequency.

6.3. Retuned PSS: frequency-domain properties

Similar to Section 4.3, for each feedback signal, PSS parameters are redesigned to meet the desired damping of 15% and the results are summarized in Table 9. The result of the system using signal $\Delta\theta_{49,50}$ emphasizes why a signal having large network modeshape is preferable. In this case, the gain selected such that $\zeta_{m1} = 15\%$ results in instability of the system (negative GM and PM). This is because at this selected gain, a complex conjugate mode moves into the right half plane of the root loci, thus rendering the system unstable.

For other properties, the results are similar to the 3-area system in Section 4.3. One important relationship is that there is a trade-off between effective gain and delay margin. Depending on the system requirements, one may prioritize one property over the other.

7. Considerations for signal selection and WADC design

7.1. Sensitivity to delays

The sensitivity function $|S_n(j\omega_n)|$ presented earlier in this study is used to evaluate the robustness of the feedback system with respect to a variation in the controller gain at the inter-area frequency [17]. In general, sensitivity studies can be extensive. It is, however, not the main focus of this paper to thoroughly explore all of them but rather to present some sensitivity studies which are relevant to the WADC design using the dominant path signals.

Table 10
Damping performance subject to delays: No contingency.

Signals	Damping ratio, ζ_{m1} (%)							
	$T_d = 0$ (ms)	100	200	300	400	500	600	700
$\Delta\theta_{7,8}$	5.68	5.51	5.31	5.06	4.79	4.50	4.19	3.89
$\Delta\theta_{6,8}$	6.30	6.07	5.77	5.43	5.06	4.65	4.23	3.81
$\Delta\theta_{5,8}$	9.12	8.56	7.87	7.06	6.16	5.21	4.24	3.29
$\Delta\theta_{4,8}$	10.67	9.96	9.05	7.95	6.73	5.44	4.14	2.89
$\Delta\theta_{3,8}$	13.00	12.06	10.80	9.25	7.51	5.67	3.86	2.16
$\Delta\theta_{2,8}$	14.06	13.05	11.64	9.88	7.86	5.74	3.66	1.75
$\Delta\theta_{1,8}$	15.00	13.95	12.43	10.47	8.19	5.78	3.45	1.35

Table 11
Sensitivity subject to delays: No contingency.

Signals	Sensitivity							
	$T_d = 0$ (ms)	100	200	300	400	500	600	700
$\Delta\theta_{7,8}$	–	1.67	2.08	2.43	2.72	2.93	3.05	3.08
$\Delta\theta_{6,8}$	–	2.36	2.92	3.40	3.79	4.06	4.20	4.23
$\Delta\theta_{5,8}$	–	5.55	6.94	8.11	8.99	9.51	9.67	9.47
$\Delta\theta_{4,8}$	–	7.13	9.17	10.92	12.20	12.90	12.99	12.51
$\Delta\theta_{3,8}$	–	9.41	12.61	15.43	17.46	18.37	18.14	16.98
$\Delta\theta_{2,8}$	–	10.16	14.06	17.61	20.18	21.25	20.76	19.10
$\Delta\theta_{1,8}$	–	10.57	15.19	19.59	22.82	24.09	23.28	21.02

Table 12
Damping performance subject to delays: Line outage.

Signals	Damping ratio, ζ_{m1} (%)							
	$T_d = 0$ (ms)	100	200	300	400	500	600	700
$\Delta\theta_{7,8}$	7.00	6.82	6.59	6.32	6.02	5.68	5.33	4.97
$\Delta\theta_{6,8}$	7.74	7.49	7.18	6.81	6.39	5.94	5.47	4.98
$\Delta\theta_{5,8}$	11.00	10.44	9.73	8.90	7.96	6.95	5.90	4.85
$\Delta\theta_{4,8}$	12.75	12.04	11.13	10.03	8.77	7.42	6.02	4.64
$\Delta\theta_{3,8}$	14.62	13.73	12.57	11.17	9.57	7.85	6.10	4.39
$\Delta\theta_{2,8}$	15.47	14.52	13.26	11.71	9.94	8.04	6.11	4.24
$\Delta\theta_{1,8}$	16.21	15.22	13.88	12.21	10.29	8.22	6.12	4.10

Table 13
Sensitivity subject to delays: Line outage.

Signals	Sensitivity							
	$T_d = 0$ (ms)	100	200	300	400	500	600	700
$\Delta\theta_{7,8}$	–	1.83	2.29	2.70	3.05	3.33	3.53	3.63
$\Delta\theta_{6,8}$	–	2.51	3.13	3.68	4.14	4.50	4.75	4.86
$\Delta\theta_{5,8}$	–	5.61	7.06	8.34	9.39	10.13	10.56	10.52
$\Delta\theta_{4,8}$	–	7.09	9.15	11.02	12.54	13.55	13.98	13.83
$\Delta\theta_{3,8}$	–	8.85	11.57	14.05	15.99	17.19	17.54	17.10
$\Delta\theta_{2,8}$	–	9.49	12.60	15.45	17.68	19.00	19.30	18.70
$\Delta\theta_{1,8}$	–	9.90	13.42	16.70	19.26	20.72	20.99	20.20

Thus, this section presents a sensitivity study of damping performance when subject to changes in time delay for the feedback system using dominant path signals as inputs.

Sensitivity computations are carried out using the 3-area study system under the nominal (*Medium*) operating condition and one contingency study (i.e. line outage). Signals along the dominant path, i.e., $\Delta\theta_{i,8}$ for $i = 1, 2, \ldots, 7$ are used as feedback inputs. For all cases, the same PSS as in Section 4.2 is installed at G_2.

7.1.1. No contingency

The damping ratios when subject to incremental time delays are presented in Table 10 (see Table 3 for PSS performance metrics). As can be expected, the damping performance degrades as the time delay increases, regardless of the input signals. When comparing within the dominant path signals, the relationship between damping performance and signal's network modeshape (see Table 2) is consistent until $T_d = 500$ ms. Observe the results in columns $T_d = 600$ and 700 ms, this relationship is no longer valid; using the signal $\Delta\theta_{1,8}$ having the largest network modeshape does not give the best damping value. This is because time delays have different impacts on different signals. To be more specific, $\Delta\theta_{1,8}$ has the smallest delay margin (comparing to other dominant path signals), thus at large T_d, the distance between the delay margin and the applied time delay is smallest, resulting in poorest damping performance.

In this study, the sensitivity to delays is calculated from the deviation in the damping ratios with respect to the incremental time delay, as described by Eq. (10)

$$\text{Sensitivity} = \frac{|\zeta_i - \zeta_{i+1}|}{\Delta\tau} \tag{10}$$

where ζ_i and ζ_{i+1} refer to the damping ratio and the adjacent one for the same input signal from Table 10 and $\Delta\tau$ refers to the difference in the amount of time delays applied. For all cases, $\Delta\tau = 0.1$ s. The computed sensitivities are presented in Table 11.

It can be seen that, for the same input signal, as the time delay increases until $T_d = 500$ ms, the sensitivity also increases. For each applied time delay, when comparing among the dominant path signals, the sensitivity is proportional to the network modeshape of a signal (see Table 2). Similar to the damping performance in Table 10, for $T_d = 600$ and 700 ms, this relationship (that the sensitivity increasing with network modeshapes) is no longer valid.

7.1.2. Contingency a: line outage

To investigate the sensitivity of delays under some contingencies, Lines 7–10 (see Fig. 2) is removed and incremental delays are applied. The damping ratios are presented in Table 12 while the sensitivities in Table 13.

The results from Table 12 agree with those from Table 10 on the damping degradation when subject to increase in time delays. Differently from the previous case, the relationship between damping performance and signal's network modeshape is not valid when $T_d = 700$ ms. Note that, when there is no delay, this contingency results in increase in damping when comparing to the *No Contingency* case (see Table 10, column $T_d = 0$ ms).

As for the sensitivity computation in Table 13, for each signal, the sensitivity increases as the time delay increases (until $T_d = 600$ ms) while, for each applied time delay, the sensitivity increases with the network modeshape of a signal.

7.1.3. Analysis

According to the case studies above, the following observations can be made:

- regardless of the choices of input signal, time delays result in damping degradation,
- for each applied time delay, the damping performance is proportional to each signal's network modeshape up to a certain amount of time delay,[7]
- for each signal, the sensitivity increases as the time delay increases up to a certain amount of time delay,
- for each applied time delay, the sensitivity increases with the network modeshape of a signal.

Then, it can be inferred that there is a trade-off between damping performance (signals having large network modeshape) and robustness (sensitivity) with regard to time delay.

[7] This depends on the contingency and how close the delay is to the delay margin of the signals.

Table 14
Control loop metrics: Signal combination, fixed PSS.

Signals	$S_{\Delta\theta}$	ζ_{m1} (%)	DM (ms)	$\lvert Sn(j\omega_n)\rvert$
$\Delta\theta_{7,8}$	0.18	5.68	N/A	0.69
$\Delta\theta_{7,8} + \Delta\theta_{6,8}$	0.44	7.83	1386.7	0.48
$\Delta\theta_{7,8} + \Delta\theta_{5,8}$	0.76	10.54	981.7	0.35
$\Delta\theta_{7,8} + \Delta\theta_{4,8}$	0.93	12.07	888.1	0.30
$\Delta\theta_{7,8} + \Delta\theta_{6,8} + \Delta\theta_{5,8}$	1.02	12.37	879.7	0.28
$\Delta\theta_{7,8} + \Delta\theta_{3,8}$	1.19	14.33	797.3	0.25
$\Delta\theta_{7,8} + \Delta\theta_{2,8}$	1.30	15.39	764.4	0.23
$\Delta\theta_{7,8} + \Delta\theta_{1,8}$	1.39	16.33	738.4	0.22
$\Delta\theta_{1,8}$	1.21	15.00	769.2	0.25
$\Delta\theta_{7,8} + \Delta\theta_{10,8}$	0.76	10.71	962.8	0.35

Table 15
Control loop metrics: Signal combination, retuned PSS.

Signals	$S_{\Delta\theta}$	K_{eff}	DM (ms)	$\lvert Sn(j\omega_n)\rvert$
$\Delta\theta_{7,8}$	0.18	5598	785.9	0.20
$\Delta\theta_{7,8} + \Delta\theta_{6,8}$	0.44	2326	783.4	0.21
$\Delta\theta_{7,8} + \Delta\theta_{5,8}$	0.76	1220	780.9	0.22
$\Delta\theta_{7,8} + \Delta\theta_{4,8}$	0.93	951	777.7	0.23
$\Delta\theta_{7,8} + \Delta\theta_{6,8} + \Delta\theta_{5,8}$	1.02	932	781.7	0.22
$\Delta\theta_{7,8} + \Delta\theta_{3,8}$	1.19	726	774.1	0.24
$\Delta\theta_{7,8} + \Delta\theta_{2,8}$	1.30	656	772.0	0.24
$\Delta\theta_{7,8} + \Delta\theta_{1,8}$	1.39	605	769.9	0.24
$\Delta\theta_{1,8}$	1.21	685	769.8	0.25
$\Delta\theta_{7,8} + \Delta\theta_{10,8}$	0.76	1135	717.3	0.24

7.2. Signal combination

Ideally, the signal having the largest network modeshape is recommended as the controller's inputs. However, such signal might not be available due to data loss. Thus, the use of multiple signals (signal combination) is proposed as an alternative to mitigate a severe degradation of a controller's performance when such incident occurs.

Effects of combining dominant path signals as feedback inputs for fixed PSS and retuned PSS studies are summarized in Table 14–15, respectively.

Fixed PSS

In Table 14, different combination of signals are implemented using the same PSS, their corresponding damping performance of Mode 1, delay margins, and sensitivity are compared.

Overall, when comparing to a single signal, using a signal combination improves the damping and the robustness (reducing the sensitivity) of the system but *reduces the delay margin*. For example, the set $\Delta\theta_{7,8} + \Delta\theta_{5,8}$ results in a higher damping ratio, higher robustness, but smaller delay margin than their individual signals when comparing to the signals $\Delta\theta_{7,8}$ or $\Delta\theta_{5,8}$ alone (see Table 3).

The set of combination to choose depends on system specifications and signal availability. Suppose only signals from Buses 5 to 8 are available and the minimum damping requirement is 10%. Then, the set of $\Delta\theta_{7,8} + \Delta\theta_{6,8} + \Delta\theta_{5,8}$ is preferred to the set of $\Delta\theta_{7,8} + \Delta\theta_{5,8}$ since their resulting delay margin is larger, thus, higher stability margin. On the other hand, if the set of three signals is implemented, when one of the signals is lost (provided that there are at least two signals), the resulting damping is still higher than using an individual signal.

Compare the set of dominant-only signals to a set of dominant and non-dominant path signals. The set $\Delta\theta_{7,8} + \Delta\theta_{5,8}$ (dominant-only) and $\Delta\theta_{7,8} + \Delta\theta_{10,8}$ (dominant and non-dominant) have similar amount of network modeshapes and robustness. However, the dominant-path only combination results in a larger delay margin though yielding slightly smaller damping ratios than the other pair. This demonstrates the capacity of a dominant path signal to accommodate more latency than the non-dominant path signal.

Retuned PSS

In Table 15, each combination of signals are implemented with each individual PSS such that $\zeta_{m1} = 15\%$. Their corresponding control effort (K_{eff}) delay margins, and sensitivity are compared.

Overall, when comparing to a single signal, using a signal combination reduces the control effort but also *reduces the delay margin* and the robustness (increasing the sensitivity). Still, the variations in the delay margin and the sensitivity are small while the reduction in control effort is significant.

Comparing the set of $\Delta\theta_{7,8} + \Delta\theta_{6,8} + \Delta\theta_{5,8}$ to the set of two signals or individual signals, the gain is greatly reduced while the delay margin is slightly decreased. On the other hand, if the combination is implemented, when a signal is lost, the delay margin is slightly increased but a significant amount of control effort is needed to maintain the same damping requirement.

Compare the set of dominant-only signals to a set of dominant and non-dominant path signals. The set $\Delta\theta_{7,8} + \Delta\theta_{5,8}$ (dominant-only) requires larger control effort but can accommodate more latency and less sensitive to gain variation than the set $\Delta\theta_{7,8} + \Delta\theta_{10,8}$ (dominant and non-dominant).

Signal combination can be practical and useful in the case of signal loss or if the selected signal's corresponding (communication and transmission) delay is too large since other signals can serve as backups. It is important to note that the allowable time delay of a signal combination will be dependent on the maximum delay among the signals. Ideally, such allowable delay should be the design specification to the communication network engineers [21]. Regardless of the latency, the controller should be able to adapt automatically according to input signals.

7.3. Controller location

System's damping improvement depends not only on the value of the network modeshape of the feedback input signal but also on the location of the controller. Many studies use residue or participation factor for controller placement [23,24]. This study uses the algorithms in [6] and place the PSS at the origin of the inter-area mode which is at one edge of the dominant path. To demonstrate the impact of PSS locations, the same PSS using the same feedback input ($\Delta\theta_{1,8}$) is placed at (i) the center of the dominant path and (ii) the other edge of the path. The study is performed on the KTH-NORDIC32 system whose dominant path is the same as in Section 6. The results are compared with the default location G_{18} and are illustrated in Fig. 12. Here the responses are the deviation in active power from Bus 38 to Bus 40 $\Delta P_{38,40}$, the PSS locations at the default, the center and the other edge are in blue, green and red, respectively. It can be seen that controller placement plays a significant role and could destabilize the system if not placed properly.

7.4. Proposed guidelines for WADC design

From the results in this study, it is recommended the use of signal combination or multi-input–single-output (MISO) scheme as a default for WADC. The multiple inputs should include those from the dominant paths having large network modeshape contents while the output of the controller should modify the voltage reference of the exciter at the location where the origin of the inter-area mode is.

The PSS to damp a specific inter-area oscillation should be placed at the origin of the mode which is usually at one edge of the dominant inter-area oscillation path.

Table 16
Signal selection comparison.

Study system	Dominant path algorithm		Residue	Participation factors	Geometric measures	
	Input signals	PSS siting			Modal observability	Modal controllability
3-area	$\Delta\theta_{1,8}$	G_2	θ_1, θ_2	ω_1, ω_2	θ_1, θ_2	G_2, G_3
KTH-NORDIC32	$\Delta\theta_{52,50}$	G_{18}	θ_{18}	ω_7, ω_2	θ_{18}, θ_{50}	G_{14}, G_{12}

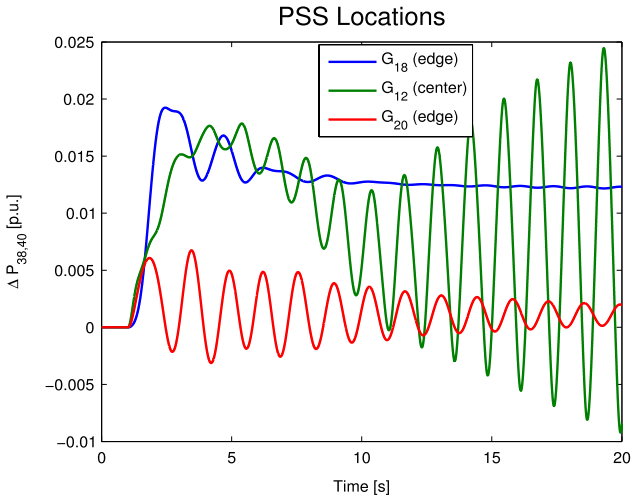

Fig. 12. Time responses of the closed loop system. (For interpretation of the references to color in this figure legend, the reader is referred to the web version of this article.)

For the PMU locations, it is recommended that the PMUs should be placed on the buses on the dominant path. If the costs are the constraint, placement on both edges of the paths are sufficient.

8. Discussions

8.1. Input signal selections: comparison with other approaches

This paper used the algorithm from [6] to identify an effective set of signals to be used as feedback inputs. This section compares the adopted algorithm with other traditional signal selection methods; namely, residue, participation factors and geometric measures of observability and controllability. Residue is a measure of both controllability and observability of the selected mode (the inter-area mode in this case) while participation factors determine which state variables are more significant for that particular mode [25]. The former is used to evaluate the effect of the location of the feedback (PSS siting) which also assumes the local signal to be used as a feedback input while the latter indicates coupling between the selected mode and state variables. The equations to compute geometric measures can be found in [26].

The comparisons are demonstrated in Table 16 where the signals having the largest (and the second largest) values for each method are presented. For the 3-area system, all the methods give similar results; the residue suggests θ_1 and θ_2 as the PSS locations and the feedback inputs while the participation factor indicates that the speed of G_1 and G_2 are most involved in this inter-area mode. θ_1 has the largest modal observability followed by θ_2 while the modal controllability of G_2 and G_3 are commensurate.[8]

For the KTH-NORDIC32 system, the residue and modal observability give similar results as the dominant path algorithm; i.e., θ_{18}.[9] The algorithm suggests θ_{50} from Bus 50 which is adjacent to G_{18}. The participation factors, however, indicate that the speed of G_7 and G_2 are most involved in this inter-area mode while G_{14} has the largest controllability followed by G_{12}.

9. Conclusion

Important properties, particularly those that relate to the network modeshape contents, of the dominant inter-area oscillation path signals have been investigated through two PSS design studies using small and large study systems and summarized here. When using the same controller, signals' network modeshapes are proportional to their respective damping capacity but are inversely proportional to the delay margins and the sensitivity to gain variation at the inter-area frequency. On the other hand, when designing a PSS to meet the same damping requirement, signals' network modeshapes are proportional to the sensitivity to gain variation at the inter-area frequency but are inversely proportional to the delay margin and the control effort. Overall, there is a trade-off between damping efficacy and system stability. In addition, it has been demonstrated that, regardless of the input signals, time delays degrade damping performance and that there is a trade-off between damping effectiveness and robustness with regard to time delays. Depending on system requirements, specifications, and resources availability, one may choose the signal of choice by assessing the two key factors: open-loop observability of the signals and delay bounds of the network.

A study on signal combination and a comparison to the non-dominant path signals have also been made. An important observation is that for a controller designed to use a specific signal (or a set of signals), a lower damping is expected if the original signal(s) is replaced by another signal due to loss of signal or large delays. Comparing to non-dominant path signals, not only the dominant path signals can achieve higher damping performance but also can accommodate larger amount of delays.

Additionally, impacts on control loop properties when subject to different loadings have been investigated. The proposed systematic relationships are more pronounced and valid in a more stressed system where the modal observability of the inter-area mode is higher. As the system is less stressed, some properties become less orderly and have different patterns. For example, in the case of *Low* scenario, retuned PSS, the network modeshapes are proportional to the delay margin which is not the case with the other two scenarios.

The selection of the "right" input signal as well as "right" control location is critical for effective damping control in WADC. The concept of dominant inter-area oscillation path is significant and useful because it lays a systematic approach for the signal selection and controller placement. Together with the results from this study, one has a comprehensive view of the choice of signal one has made and the consequences of the impacts such signal has on different properties of the control loop.

The analysis of varying (stochastic) time delays requires the simulation of a hybrid automata which is limited by the simulation software used in this study. However, time delay modeling is not the main focus of this study but rather the relationship with and its impacts on the network modeshape of the signals on the dominant inter-area oscillation path.

8 G_1 is not listed because the generator is a classical model.

9 In the dominant path algorithm, only the signals from high-voltage buses are considered.

Acknowledgments

Y. Chompoobutrgool is supported by Elforsk, Sweden. L. Vanfretti is supported by Statnett SF, the NER-funded STRONgrid project and the STandUP for Energy collaboration initiative.

Appendix. Damping ratio and loadings relationship

Inter-area oscillations, as well as other electromechanical modes, can be approximately obtained from electromechanical model

$$\begin{bmatrix} \Delta\dot{\delta} \\ \Delta\dot{\omega} \end{bmatrix} = \begin{bmatrix} \omega_0 & 0 \\ -\frac{K_D}{2H} & -\frac{K_S}{2H} \end{bmatrix} \begin{bmatrix} \Delta\delta \\ \Delta\omega \end{bmatrix} + Bu \tag{A.1}$$

where ω_0 is the rated speed, H is the machine inertia, K_D is the damping coefficient and K_S is the synchronizing coefficient. Rearranging and having rotor angle δ as the state variable, the characteristic equation is given by

$$s^2 + \frac{K_D}{2H}s + \frac{K_S\omega_0}{2H} = 0 \tag{A.2}$$

which is of the general form

$$s^2 + 2\zeta\omega_n s + \omega_n^2 = 0 \tag{A.3}$$

where ω_n is the undamped natural frequency. From (A.3), the damping ratio ζ is

$$\zeta = \frac{1}{2}\frac{K_D}{\sqrt{K_S 2H\omega_0}}. \tag{A.4}$$

All equations are taken from [27]. Since H and ω_0 are the same for all three operating conditions, changes in K_D and K_S can be used to associate the change in damping ratio to the change in loadings. The inter-area mode of interest is between Area B and C, thus, only elements associated with G_1 and G_2 are considered.

From (A.1), K_D is the same for all cases while the matrix norms for K_S for each case are $|K_{S,High}| = 0.00027$, $|K_{S,Nominal}| = 0.00057$, and $|K_{S,Low}| = 0.0007$. From (A.4), this explains why damping performance is largest in *High* loading and smallest in *Low* loading.

References

[1] W. Sattinger, Application of PMU measurements in Europe: TSO approach and experience, in: IEEE Trondheim PowerTech 2011, June 2011, pp. 1–4.
[2] M.E. Aboul-Ela, A.A. Sallam, J.D. McCalley, A.A. Fouad, Damping controller design for power system oscillations using global signals, IEEE Trans. Power Syst. 11 (2) (1996) 767–773.
[3] J.H. Chow, J.J. Sanchez-Gasca, H. Ren, S. Wang, Power system damping controller design using multiple input signals, IEEE Control Syst. Mag. (2000) 82–90.
[4] G.E. Boukarim, S. Wang, J.H. Chow, G.N. Taranto, N. Martins, A comparison of classical, robust, and decentralized control designs for multiple power system stabilizers, IEEE Trans. Power Syst. 15 (4) (2000) 1287–1292.
[5] I. Kamwa, R. Grondin, Y. Hebert, Wide-area measurement based stabilizing control of large power systems—a decentralized/hierarchical approach, IEEE Trans. Power Syst. 16 (1) (2001) 136–153.
[6] Y. Chompoobutrgool, L. Vanfretti, Identification of power system dominant inter-area oscillation paths, IEEE Trans. Power Syst. 28 (3) (2013) 2798–2807.
[7] Y. Chompoobutrgool, L. Vanfretti, A fundamental study on damping control design using PMU signals from dominant inter-area oscillation paths, in: North American Power Symposium, NAPS, 2012, September 2012, pp. 1–6.
[8] D. Dotta, A.S. e Silva, I.C. Decker, Wide-area measurements-based two-level control design considering signal transmission delay, IEEE Trans. Power Syst. 24 (1) (2009) 208–216.
[9] B. Chaudhuri, R. Majumder, B.C. Pal, Wide-area measurement-based stabilizing control of power system considering signal transmission delay, IEEE Trans. Power Syst. 19 (4) (2004) 1971–1979.
[10] J.W. Stahlhut, T.J. Browne, G.T. Heydt, V. Vittal, Latency viewed as a stochastic process and its impact on wide area power system control signals, IEEE Trans. Power Syst. 23 (1) (2008) 84–91.
[11] N.R. Chaudhuri, S. Ray, R. Majumder, B. Chaudhuri, A new approach to continuous latency compensation with adaptive phasor power oscillation damping controller (POD), IEEE Trans. Power Syst. 25 (2) (2010) 939–946.
[12] W. Yao, L. Jiang, Q.H. Wu, J.Y. Wen, S.J. Cheng, Delay-dependent stability analysis of the power system with a wide-area damping controller embedded, IEEE Trans. Power Syst. 26 (1) (2011) 233–240.
[13] H. Wu, K.S. Tsakalis, G.T. Heydt, Evaluation of time delay effects to wide-area power system stabilizer design, IEEE Trans. Power Syst. 19 (4) (2004) 1935–1941.
[14] Y. Chompoobutrgool, L. Vanfretti, Analysis of time delay effects for wide-area damping control design using dominant path signals, in: IEEE Power and Energy Society General Meeting, 2012, July 2014, pp. 1–8.
[15] J.F. Hauer, D.J. Trudnowski, J.G. DeSteese, A perspective on WAMS analysis tools for tracking of oscillatory dynamics, in: IEEE PES General Meeting, 2007.
[16] L. Mirkin, Z.J. Plamor, Control issues in systems with loop delays, in: Handbook of Networked and Embedded Control Systems, Birkhäuser, 2005, (Chapter).
[17] D. Frederick, J. Chow, Feedback Control Problems using MATLAB and the Control System Toolbox, in: BookWare Companion Series, 2000.
[18] Y. Chompoobutrgool, L. Vanfretti, On the persistence of dominant inter-area oscillation paths in large-scale power networks, in: Proceedings of 8th IFAC Symposium on Power Plants and Power Systems, Toulouse, France, September 2012.
[19] Jaw-Kuen Shiau, G.N. Taranto, J.H. Chow, G. Boukarim, Power swing damping controller design using an iterative linear matrix inequality algorithm, IEEE Trans. Control Syst. Technol. 7 (3) (1999) 371–381.
[20] J.H. Chow, S. Ghiocel, An adaptive wide-area power system damping controller using synchrophasor data, in: Control and Optimization Methods for Electric Smart Grids, in: Springer Series in Power Electronics and Power Systems, 2012, (Chapter).
[21] N.T. Anh, L. Vanfretti, J. Driesen, D. Van Hertem, A quantitative method to determine ICT delay requirements for wide-area power system damping controllers, IEEE Trans. Power Syst. PP (99) (2014) 1–8.
[22] Y. Chompoobutrgool, Wei Li, L. Vanfretti, Development and implementation of a Nordic grid model for Power System small-signal and transient stability studies in a free and open source software, in: IEE Power and Energy Society General Meeting, July 2012, pp. 1–8.
[23] A.F. Snyder, N. Hadjsaid, D. Georges, L. Mili, A.G. Phadke, O. Faucon, S. Vitet, Inter-area oscillation damping with power system stabilizers and synchronized phasor measurements, in: Proceedings of International Conference on Power System Technology, vol. 2, POWERCON '98, 1998, pp. 790–794.
[24] Graham Rogers, Power System Oscillations, Kluwer Academic Publishers, Norwell, MA, 1999.
[25] F. Luis Pagola, Ignacio J. Perez-Arriaga, George C. Verghese, On sensitivities, residues and participations: Applications to oscillatory stability analysis and control, IEEE Trans. Power Syst. 4 (1) (1989) 278–285.
[26] A.M.A. Hamdan, A.M. Elabdalla, Geometric measures of modal controllability and observability of power system models, Electr. Power Syst. Res. 15 (1988) 147–155.
[27] P. Kundur, Power System Stability and Control, in: The EPRI Power System Engineering Series, McGraw-Hill, 1994.